Modeling of compound semiconductors: Analytical bond-order potential for Ga, As, and GaAs

Karsten Albe*
University of Illinois at Urbana-Champaign, Frederick Seitz Materials Research Laboratory, 104 South Goodwin Avenue, Urbana, Illinois 61801

Kai Nordlund and Janne Nord
University of Helsinki, Accelerator Laboratory, P. O. Box 43, FIN-00014 University of Helsinki, Finland

Antti Kuronen
Helsinki University of Technology, Laboratory of Computational Engineering, P. O. Box 9400, FIN-02015 Helsinki, Finland
(Received 11 July 2001; published 26 July 2002)

An analytical bond-order potential for GaAs is presented, that allows one to model a wide range of properties of GaAs compound structures, as well as the pure phases of gallium and arsenide, including nonequilibrium configurations. The functional form is based on the bond-order scheme as devised by Abell-Tersoff and Brenner, while a systematic fitting scheme starting from the Pauling relation is used for determining all adjustable parameters. Reference data were taken from experiments if available, or computed by self-consistent total-energy calculations within the local density-functional theory otherwise. For fitting the parameters, only structural data of the metallic phases of gallium and arsenide as well as those of different GaAs phases were used. A number of tests on point defect properties, surface properties, and melting behavior have been performed afterward in order to validate the accuracy and transferability of the potential model, but were not part of the fitting procedure. While point defect properties and surfaces with low As content are found to be in good agreement with literature data, the description of As-rich surface reconstructions is not satisfactory. In the case of molten GaAs we find support for a structural model based on experiment that indicates a polymerized arsenic phase in the melt.

DOI: 10.1103/PhysRevB.66.035205 PACS number(s): 61.50.Ah, 61.20.Ja, 81.05.Ea, 61.50.Lt

I. INTRODUCTION

Compound semiconductors, such as GaAs, are of increasing technological importance because of their use in optoelectronic applications and also because of their potential to replace silicon in microelectronic components which require a high carrier mobility.[1] As the use of compound semiconductors becomes more widespread, the interest in using ion implantation in their processing also has increased, and is now used for instance in the fabrication of GaAs-based MOSFETs[2] Even though GaAs is probably the most studied compound semiconductor, many aspects of materials processing like radiation damage or surface growth are not fully understood. Diffuse x-ray scattering work has elucidated the mechanisms of point defect production by electrons in GaAs,[3] and defect recovery and amorphization by ion irradiation is also fairly well understood.[4,5] But many details of the initial damage production process by ions and subsequent damage clustering remain poorly understood. Moreover, since GaAs components are frequently manufactured by various surface growth methods,[1] the properties of the GaAs surfaces during intermediate growth stages are also of great scientific interest.

Understanding and improving these manufacturing steps, which are typically driven by physical processes far from equilibrium, is therefore a task of high technological importance. A natural tool for studying irradiation effects and processes like surface growth are atomistic computer simulations. Molecular dynamics (MD) as well as kinetic Monte Carlo (MC) method have become key tools for modeling material processes based on an atomic level description.

However, in both MC and MD simulations it is not feasible to calculate the Hamiltonian by means of quantum-mechanical methods because of their enormous computational demands. Therefore analytical potentials that provide a sufficiently accurate approximation of the energy hypersurface are an indispensable tool for large-scale computer simulation studies. Such potentials have been very successfully used in the past for simulations of covalent materials like silicon, carbon, and others, as well as numerous metals and alloys (see, e.g., Refs. 6–9), but much less for compound semiconductors. This is because of the difficulties in modeling the interatomic interaction in semiconducting compound materials and its constituents by means of a simplified approximative analytical functional that has to be valid not only for equilibrium but also nonequilibrium configurations.

Ito, Khor, and Das Sarma were the first to propose a bond-order-type potential for GaAs.[10] However, since no parameter sets for the pure elements were given, this model cannot be used for simulations of nonequilibrium processes. Smith[11] proposed a complete Tersoff-like potential for GaAs that was later modified in a study by Sayed *et al.*[12] These potentials have problems in describing surfaces, melting behavior, point defects and pure structures and are therefore restricted in their applicability.[13] Recently, Conrad and Scheerschmidt[14] published a potential with parameters directly derived from the tight-binding momentum approximation. Although this potential is theoretically better motivated, it suffers from problems similar to those mentioned above.

Most seriously, the potential predicts a positive heat of formation for the zinc-blende structure, that leads to a phase decomposition of GaAs after heating and cooling. While the Smith and Sayed *et al.* potentials are only fit to a limited set of reference data, the problems of the potentials of Ref. 14 might be related to an inappropriate set of tight-binding parameters, that has been used for the parametrization. A different approach was chosen by Kodiyalam *et al.*[15] for studying phase transformations in GaAs nanoclusters. They combined an electrostatic term and a Stillinger-Weber three-body function, but did not include bond-order dependencies or charge-transfer effects. Therefore, only processes that do not include changes of the chemical environment can be realistically described with this scheme.

In the present study we have explored the possibility to devise a potential that overcomes the deficiencies of the existing models and is sufficiently transferable. Our criteria included the description of various crystalline structures of the elements and the compound system, their melting behavior, point defect and surface properties.

In fact after almost two decades of efforts in developing analytical potentials for solid structures, there is still no general recipe for how to achieve this. However, in our opinion there are three indispensable key ingredients of equal importance. First, a well-motivated analytical form has to be derived, that is simple but not oversimplifying. Second, the parameters have to be adjusted using a solid and systematic fitting procedure. Finally, a reference data set as large as possible is necessary, which should be taken from experiments and quantum mechanical total-energy calculations. In this study we have made an attempt to derive a potential that fulfills these requirements and delivers an energy description for a wide range of configurations of Ga, As, and GaAs.

The paper is organized as follows. First we give the analytical form of the bond-order potential as used in this study, and explain the strategy for its parametrization. Then the technical details of the total energy calculations are briefly described and the parameter sets for pure Ga, pure As, and GaAs are derived and discussed in detail. Finally, we give a series of examples that prove the transferability of the given potential.

II. BASIC METHODOLOGY AND ENERGY FUNCTIONAL

Gallium arsenide is a semiconducting material with dominantly covalent bonds. Due to the small difference in electronegativities of about 0.4, local charge transfer leads to interacting effective net charges. Pure gallium and pure arsenide structure have mixed covalent and metallic bonds, as discussed below in detail. Consequently, an analytical potential for GaAs would ideally be able to deal with all those types of chemical bonds. To our knowledge there is presently no established scheme for a reactive analytical potential that fulfills these requirements. Only the numerically expensive variable charge method proposed by Streitz and Mintmire for modeling mixed ionic-metallic interaction[16] would be a possible candidate, but hitherto this has only been parametrized for a small number of metal oxides without considering explicitly angular terms.

In our approach we have therefore adopted a short-ranged bond-order potential similar to the Tersoff-Brenner type. This ansatz allows us, in principle, to model covalent and metallic bonds within one functional form.[17] Although long-range interactions are not explicitly included, the use of a short-ranged potential for modeling the ionic-covalent interaction in GaAs can be justified because the Madelung energies for this compound are small compared to the covalent binding energy, and moreover are implicitly included in the input data set as taken from experiment or density-functional-theory (DFT) calculations.

Following Tersoff and Brenner,[17] the total potential energy is written as a sum over individual bond energies:

$$E=\sum_{i>j} f_{ij}(r_{ij})\left[V_{ij}^{R}(r_{ij}) - \underbrace{\frac{B_{ij}+B_{ji}}{2}}_{\overline{B_{ij}}} V_{ij}^{A}(r_{ij}) \right]. \quad (1)$$

The pairlike attractive and repulsive energies are given in Morse-like forms

$$V^{R}(r)=\frac{D_o}{S-1}\exp[-\beta\sqrt{2S}(r-r_o)],$$

$$V^{A}(r)=\frac{SD_o}{S-1}\exp[-\beta\sqrt{2/S}(r-r_o)], \quad (2)$$

that depend on the dimer bond energy D_o, the dimer bond distance, and the adjustable parameter S. The parameter β can be determined by the ground-state oscillation frequency of the dimer. The major caveat of this ansatz is the finite repulsion at interatomic distances approaching zero. If necessary, this can be corrected by a spline procedure, as described in the Appendix.

Since we only consider the bond integrals to the next neighbors, it is convenient and computationally efficient to restrict the interaction to the next neighbor sphere by a cutoff-function

$$f(r)=\begin{cases} 1, & r\leqslant R-D \\ \frac{1}{2}-\frac{1}{2}\sin\{\pi(r-R)/(2D)\}, & |R-r|\leqslant D \\ 0, & r\geqslant R+D, \end{cases} \quad (3)$$

where D and R are adjustable quantities.

The bond-order parameter $\overline{B_{ij}}$ also includes angular dependencies, which are necessary to accurately model the deformation of covalent bonds. Tersoff proposed an angular-dependent bond-order function for silicon, carbon, and germanium,[18] while Brenner introduced a more refined approach[19] for modeling hydrocarbons. Other closely related potentials were proposed for Si and C,[20] and, recently, several studies derived analytical bond-order functions directly from a momentum expansion.[14,21,22] Although all of these approaches differ in the details of their functional form, the resulting angular dependencies of the bond order are proven to be very similar.[22,23] Therefore we have adopted a straightforward extension as used by Brenner, which is simply an

angular-dependent term $g(\theta)$ in the inner sum of the bond-order function, so that B_{ij} reads

$$B_{ij}=(1+\chi_{ij})^{-1/2},$$

$$\chi_{ij}=\sum_{k(\neq i,j)} f_{ik}(r_{ik})g_{ik}(\theta_{ijk})\exp[2\mu_{ik}(r_{ij}-r_{ik})]. \quad (4)$$

Here again the cutoff function is included, while the indices monitor the type dependence of the parameters, which is important for a description of compounds. The square root dependence of the bond order is chosen in agreement to the second-order momentum approximation and is not subject to adjustments in the fitting procedure. The angular function $g(\theta)$ is given by

$$g(\theta_{ijk})=\gamma\left(1+\frac{c^2}{d^2}-\frac{c^2}{[d^2+(h+\cos\theta_{ijk})^2]}\right). \quad (5)$$

For $c=0$ this term vanishes and the total potential resembles a short ranged embedden-atom-method potential of the Finnis-Sinclair type.[17]

Despite the semiempirical character of this approach, the number of freely adjustable parameters is not more than six for each interaction type. If the binding energy D_o and the ground-state frequency of the dimer molecule are known, then β is simply given by

$$\beta=k\frac{2\pi c}{\sqrt{2D_o/\mu}}, \quad (6)$$

where k is the wave number and μ the reduced mass.

The parameter S can be determined by the Pauling relation, which connects the equilibrium bonding distance r_b and the energy per individual bond E_b:

$$E_b=-D_o\exp[-\beta\sqrt{2S}(r_b-r_o)]. \quad (7)$$

In order to reproduce the lattice parameters and cohesive energies of structures with different atomic coordinations, the condition in Eq. (7) has to be fulfilled. Only then can we expect the potential to be transferable to structural configuration that are not part of the input data base.

III. TOTAL-ENERGY CALCULATIONS

Where necessary, reference data for the potential fitting were computed from total energy calculations in the framework of the density functional theory[24] with the pseudopotential code CASTEP.[25] Ultrasoft pseudopotentials (us-PP) as given by Lee were applied and the local-density approximation (LDA) (Refs. 26 and 27) was taken for exchange and correlation functionals. For all calculated structures the cutoff energies and k points were chosen to achieve convergence better than 0.01eV/atom. For the pure structures the experimental and several hypothetical structures were calculated. The minimum total energy, lattice constant, bulk modulus, and pressure derivative of the bulk modulus were calculated from energy-volume data by fitting to the Birch-Murnaghan equation.[28,29]

IV. FITTING PROCEDURE

The parameter set for Ga-Ga, As-As, and Ga-As were adjusted independently. Those structures and properties, that are affected by the interplay of the different parameters, were not included in the fitting procedure, but were analyzed later. The parameters in the pairlike terms were chosen in accordance to the dimer properties if possible, while the slope of the energy-bond relation was adjusted to the total energy data by varying S. Finally, elastic moduli and structural properties were fitted simultaneously using the Levenberg-Marquardt method.[30]

A. Gallium

Gallium has a rather complicated phase diagram with many stable and metastable crystalline phases, all close in energy to the ground state.[41] The stable low-pressure phase α-Ga reveals an unusual crystal structure. It can be described in terms of a face-centered orthorhombic cell with each site occupied by a Ga_2 dimer. The semimetallic element exhibits covalent-metallic duality in its bonds. Throughout the literature cell parameters are assigned in different ways. Here we follow the definition as described in Ref. 42 with the unit-cell parameter b corresponding to the long axis. One atom is located at $(0,u,v)$ with $u=0.1539$ and 0.0798 in fractional coordinates of the unit cell.[32] Each atom has seven nearest neighbors, six within the distance of metallic bonds ($M1$, $M2$, $M3$) and one within a shorter distance determined by the dimerlike covalent bond (D). At higher pressures Ga-II and Ga-III are the stable configurations. The first is a body-centered structure with six atoms per unit cell, and the latter a faced-centered tetragonal structure similar to indium that appears at very high pressures (>30 kbar) and resembles a distorted fcc-lattice.

In the past, comprehensive studies of the energetics of Ga polymorphs using DFT calculations were presented by Bernasconi and co-workers.[43,40] We performed similar calculations on α-Ga, Ga-II, fcc-Ga, and the hypothetical diamond as well as the simple cubic structure. The anisotropic α-Ga has three independent lattice parameters and two internal degrees of freedom. We minimized the total energy by varying the cell parameters to achieve zero stresses. The internal coordinates were kept fixed at the experimental value during this step. Afterward, the internal coordinates were relaxed leading to a remaining residual stress of less than 1 kbar. In Table I the calculated structural parameters are given. In general, LDA results underestimate the lattice parameters. However, our calculations with ultrasoft pseudopotentials are in better agreement with the experimental numbers than those of Bernasconi *et al.*[40] Since DFT calculations are reliable with respect to energy differences but do not give correct cohesive energies, we have shifted the total energy of α-Ga to the experimentally known cohesive energy, and calculated all other cohesive energy from the total-energy difference of the competing structures. The energies reported by Bernasconi *et al.*[40] are in excellent agreement with our calculations for fcc and Ga-II (see Table I and Fig. 1). Even the bulk modulus for α-Ga, that we calculated for simplicity from isotropic deformations, agrees well with the value given by

TABLE I. Energy and structure of different Ga phases. Given are the experimental numbers (Refs. 31–35), theoretical dimer properties (Refs. 36–39), results of LDA calculations by the Trieste group (Ref. 40), the us-PP LDA calculations of this work, and the corresponding numbers as described with the analytical model.

	Experiment	Theory	us-PP LDA	Anal. Pot.
Ga_2	(Ref. 31)	(Refs. 36–39)		
r_o (Å)	-	2.694–2.746		2.3235
D_o (eV)	1.4	1.12–1.28		1.4
ω_o (cm^{-1})	165	162–180		162
diamond-Ga				$B_{ij}=0.9882$
V (Å^3/atom)			22.91(2)	21.22
a_o (Å^3)			5.680	5.537
r_o (Å^3)			2.459	2.397
E_{coh}/atom (eV)			−2.458	−2.485
E_{bond} (eV)			−1.2292	−1.2425
B (GPa)			46.5(2)	27.9
B'			5.06(4)	3.41
sc-Ga				$B_{ij}=0.9569$
V (Å^3/atom)			18.123	17.561
a_o (Å)			2.626	2.599
r_o (Å)			2.626	2.599
E_{coh}/atom (eV)			−2.699	−2.694
E_{bond} (eV)			−0.899	−0.898
B (GPa)			61.3(1)	42.97
B'			5.02(2)	3.36
α-Ga ($Cmca$)	(Ref. 32)	LDA (Ref. 40)		
V (Å^3/atom)	19.58	17.58	18.45	19.19
a_o (Å)	4.5192	4.3768	4.4422	4.4113
b_o (Å)	7.6586	7.3880	7.5180	7.4037
c_o (Å)	4.5258	4.3505	4.4220	4.7028
u	0.1539	0.1567	0.1558	0.1613
v	0.0798	0.0803	0.0831	0.0898
r_o (Å) D	2.4655	2.4185	2.4552	2.5339
$M1$	2.6995	2.5753	2.6257	2.6709
$M2$	2.7348	2.6399	2.6668	2.6931
$M3$	2.7918	2.6791	2.7348	2.7024
E_{coh}/atom (eV)	−2.810 (Ref. 33)[a]	−2.810[a]	−2.810[a]	−2.833
E_{bond} (eV)				
B (GPa)	61.3 (Ref. 34)	66.9	67.4(2)	42.9(4)
(@273 K)	56.9 (Ref. 33)			
B'		4.683	5.27	3.47(7)
T_{melt} (K)	302.9 (Ref. 33)	-		600(100)
Ga-II ($I\bar{4}3d$)	(Ref. 35)			$B_{ij}=0.9322$
V (Å^3/atom)	17.56	16.15	17.13	17.18
a_o (Å)	5.951	5.787	5.901	5.907
r_o (Å)	2.78	2.71	2.76	2.763

TABLE I. (*Continued*.)

	Experiment	Theory	us-PP LDA	Anal. Pot.
E_{coh}/atom (eV)		−2.752	−2.784	−2.758
E_{bond} (eV)		−0.688	−0.696	−0.689
B (GPa)		67.6	66.8(1)	50.51
B'		5.034	4.86(1)	3.749
Ga_2	(Ref. 31)	(Refs. 36–39)		
fcc-Ga				(B_{ij} = 0.8950[b])
V (Å^3/atom)		16.07	17.12(1)	16.77(19.28[b])
a_o (Å)		4.006	4.09	4.063(4.25[b])
r_o (Å)		2.83	2.89	2.87(3.01[b])
E_{coh}/atom (eV)		−2.737	−2.756	−2.711(−2.745[b])
E_{bond} (eV)		−0.456	−0.459	−0.451(−0.457[b])
B (GPa)		63.7	65.2(1)	(52.75[b])
B'		4.14	4.76(1)	(4.05[b])

[a]The total energy for this structure was shifted to the experimental cohesive energy. All other total energies were treated accordingly.

[b]Calculated under the assumption that only the first neighbor shell is within the cutoff radius.

the former work, where the axes were varied independently for each volume. Additionally, we have investigated the sc and diamond structure in order to represent configurations with low coordinations as they can typically occur around vacancies and surfaces. All structures are stable with respect to isotropic expansion and compression. It should be noted, however, that we did not investigate the stability with respect to shear deformation of the artificial simple cubic and zinc-blende structure, since only the bond strengths and lengths are of interest for the potential fitting.

The parametrization for the Ga interaction starts with the pairlike term. After having calculated the values for D_o, r_o, and β, the parameter S is in principle the only one that needs to be adjusted.

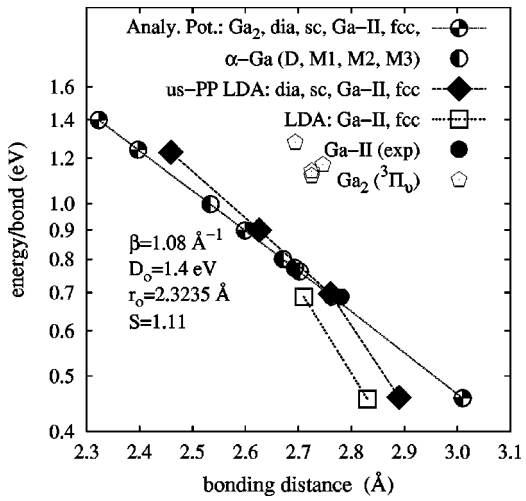

FIG. 1. Semilogarithmic plot of the energy-bond relation for different Ga structures: Shown are results of the analytical potential, the us-PP LDA calculations, and literature values of LDA calculations (Ref. 40). The experimental numbers for Ga-II are taken from Ref. 35. The calculated dimer properties are results from Refs. 36–39.

The experimental number for the Ga_2 dimer binding energy of $D_o = 1.4$ eV as given by Huber and Herzberg[31] is somewhat larger than the theoretical predictions for the $^3\Pi_u$ ground state (1.12–1.28 eV),[36–39] while no experimental value is accessible for the bond distance. Therefore, we have taken D_o in agreement with the experimental value and adjusted r_o, so that the best fit of all other reference data can be achieved (Fig. 1). The parameter β was chosen to be 1.08 (Å^{-1}), which corresponds to a wave number for the ground-state frequency of 162 cm^{-1}, in agreement with experiment and theoretical predictions.

The slope of the energy-bond relation [Eq. (7)] was then adjusted by varying the parameter S. Figure 1 shows the bond strength vs bond-length data for all Ga structures considered here, and the values as given by the analytical potential with $S = 1.11$.

Finally, the angular parameters were fitted to reproduce the structural information and the energetics of all structures as given in Table I. Using the Levenberg-Marquardt scheme all properties were adjusted with a simultaneous fitting procedure.

Describing the properties of the α-Ga structure with this relatively simple analytical potential is a nontrivial task. In general, the bond-order function acts as a local detector, that determines the bond strengths and lengths only from the structural environment. Since metallic- and covalent-type bonds in Ga are characterized by unique bond angles and distances, the algorithm is potentially able to distinguish the bond types only from the structural geometry. In the fitting procedure we have considered each bond in α-Ga individually, using the structural parameters as given by the experimental data. As can be seen from Table I, all cell parameters

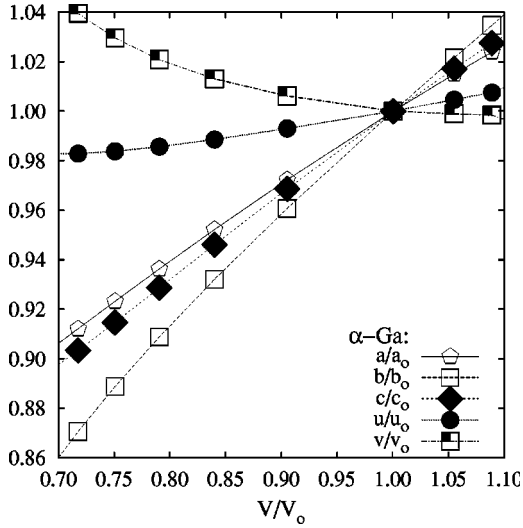

FIG. 2. Variation of α-Ga cell parameters relative to the equilibrium at different volumes calculated with the analytical potential.

as calculated with the analytical potential are in reasonable agreement with the experimental numbers. The potential is able to distinguish between the short covalent and longer metallic bonds, which proves the flexibility of the analytical scheme. Although the covalent bond is larger and the metallic bonds are shorter than the reference data, the general feature of increasing lengths $D<M1<M2<M3$ is well reproduced. In accordance with experiment, the lattice parameter a is predicted to be shorter than c, while DFT calculations erroneously predict the reverse situation. In a first application the structural parameters of α-Ga were calculated for different cell volumes by applying hydrostatic pressure. As can be seen in Fig. 2 the relative compression for the long b axis is significantly larger than for the short axes a and c. While the internal parameter u decreases almost linearly with decreasing volume, an exponential increase for v/v_o can be observed.

For all crystalline structures the agreement of the analytical model with the experimental and theoretical reference data is good in energies and bond length, while the bulk moduli are consistently too small. This is related to the choice for the parameter β, which was determined from the dimer ground-state frequency and determines the curvature of the effective pair potential.

The range of the potential is restricted to the first-neighbor shell. In determining the melting point of the α-Ga we found that a narrow cutoff interval increases the melting point. The corresponding parameters were obtained using the procedure described in Sec. V A. The optimized cutoff range of 2.8–3.1 Å leads to a second-neighbor interaction in the fcc structure, which at the same time improves the agreement of the structural parameters with the reference data (see Table I). The full parameter set is given in Table II.

B. Arsenic

The stable phase of arsenic is the rhombohedral α phase, that occurs in the $A7$ structure typical for group-V elements.

TABLE II. Parameter sets for the three interaction types.

ij	Ga-Ga	As-As	Ga-As
γ	0.007 874	0.455	0.0166
S	1.11	1.86	1.1417
β (Å^{-1})	1.08	1.435	1.5228
D_o (eV)	1.40	3.96	2.10
R_o (Å)	2.3235	2.1	2.35
c	1.918	0.1186	1.29
d	0.75	0.1612	0.56
$h=\cos(\theta_o)$	0.3013	0.077 48	0.237
2μ (Å^{-1})	1.846	3.161	0.0
R_{cut} (Å)	2.95	3.4	3.1
D (Å)	0.15	0.2	0.2

This structure can be derived from the simple cubic structure by rhombohedral shear and a relative displacement along the [111] direction. A significant feature is the presence of double layers, in which each atom has three nearest neighbors along orthogonal directions and three more at a larger distance in the neighboring layers. The α arsenic is completely characterized by the rhombohedral angle α, the lattice parameter a_o, and the internal displacement parameter u (see Table III).

In the past the rhombohedral to simple-cubic phase transition has been the subject of several theoretical[44–46,49,50] and experimental[47,48] studies. A comprehensive set of experimental data, however, exist only for the rhombohedral structure and we are only aware of one study, that has additionally studied bcc-As.[49] In this work we have therefore calculated the structural properties of As in diamond, rhombohedral, sc, bcc, and fcc structures, in order to derive a consistent data set of configurations with different coordinations.

Similar to the calculations of α-Ga, we first optimized the cell structure by keeping the internal coordinates fixed, and afterward optimized the atomic positions with a fixed cell geometry. The rhombohedral angle and the internal relaxation parameter agree very well the pseudopotential calculations performed by Needs *et al.*,[45,46] while the lattice constant is somewhat lower. More importantly the energy difference of the rhombohedral to the sc-phase is 0.069 eV and therefore exactly the same value Mattheiss *et al.*[44] reported from their linear augmented plane-wave (LAPW) calculations. In a later study Needs *et al.*[46] recalculated the sc structure with better convergence criteria, and obtained a similar energy difference of 0.06 eV. Table III gives an overview of all results in comparison. Here it should be noted, that Mattheiss *et al.*[44] calculated the cohesive energy using their LAPW scheme. The large difference in their numbers from the experimental value reflects the difficulties in obtaining reliable results for cohesive energies from total energy calculations. The bulk modulus as calculated in this work and as given by Mattheiss *et al.* is almost 50% higher than the experimental one. This is given by the fact that we did not vary the internal displacement parameter and the rhombohedral angle while changing the volumes. The numbers are therefore only given for reasons of completeness. The

TABLE III. Energy and structural parameters of different As phases. Given are experimental values and theoretical results from DFT calculations in comparison to the us-PP LDA results of this work and the corresponding numbers as described with the analytical model.

	LAPW	LDA	Exper.	us-PP LDA	Anal. Pot.
As_2			(Ref. 31)		
r_o (Å)			2.1026		2.1
D_o (eV)			3.96		3.96
ω_o (cm^{-1})			347		347
diamond-As					$B_{ij}=0.5878$
V (Å^3/atom)				25.84(2)	24.49
a_o (Å^3)				5.913	5.808
r_o (Å^3)				2.560	2.515
E_{coh}/atom (eV)				−2.487	−2.510
E_{bond} (eV)				−1.243	−1.255
B (GPa)				52.6(1)	47.22
B'				3.47(2)	4.55
α-As	(Ref. 44)	(Refs. 45, 46)	exp.		
V (Å^3/atom)	21.79	21.3	21.51	19.38	18.48
a_o (Å^3)	4.084	4.017	4.132	3.956	3.909
α (deg)	55.9	56.28	54.12	56.71	54.62
u	0.2294	0.230	0.227	0.2317	0.2321
r_o (Å^3)			2.52	2.49	2.45
			3.11	2.92	2.88
E_{coh}/atom (eV)	−(3.78)	−2.96[a]	−2.9 (Ref. 33)	−2.96[a]	−2.965
E_{bond} (eV)					
B (GPa)	(77)[b]	43	55.6 (Ref. 47)	(82.2)[b]	68.4(2)
			58(5) (Ref. 48)		
B'			3.3–4.4	4.1(1)	8.7(3)
T_{melt} (K) [c]			1090 K		$<$1200 K
sc-As			LDA (Ref. 49)		$B_{ij}=0.5199$
V (Å^3/atom)	20.05	19.25	19.28	18.48	17.8
a_o (Å^3)	2.717	2.67	2.68	2.64	2.611
r_o (Å^3)	2.717	2.67	2.68	2.64	2.611
E_{coh}/atom (eV)	−(3.711)	−2.9	−2.9	−2.89	−2.89
E_{bond} (eV)		−0.966	−0.966	−0.963	−0.963
B (GPa)	87	122	91.4	96.8(13)	80.82
B'		2.32	3.81	3.8(2)	4.64
bcc-As					$B_{ij}=0.4228$
V (Å^3/atom)			18.16	17.35	16.39
a_o (Å^3)			3.31	3.26	3.20
r_o (Å^3)			2.869	2.825	2.772
E_{coh}/atom (eV)			−2.65	−2.562	−2.462
E_{bond} (eV)			0.664	−0.640	−0.615
B (GPa)			100.97	96.8	84.39
B'			3.58	3.8	4.93

TABLE III. (*Continued*.)

	LAPW	LDA	Exper.	us-PP LDA	Anal. Pot.
fcc-As					$B_{ij}=0.3511$
V (Å^3/atom)				17.57	17.55
a_o (Å^3)				4.217	4.125
r_o (Å^3)				2.918	2.917
E_{coh}/atom (eV)				−2.442	−2.471
E_{bond} (eV)				−0.407	−0.411
B (GPa)				93(2)	87.47
B'				3.6(3)	5.10

[a]Total energy for this structure was shifted to the experimental cohesive energy. All other total energies were treated accordingly.

[b]Calculated with fixed rhombohedral angle and fixed internal coordinates.

[c]Experimental value measured at a high pressure. The simulated temperature gives the boiling point.

properties calculated for the bcc-structure are in good agreement with the numbers given by Sasaki *et al.*[49] The us-PP LDA calculation predicts a somewhat lower lattice constant and differs by 0.088 eV in the cohesive energy.

The adjustment of the potential parameters (Table II) starts again with the dimer properties. These are very important for simulating growth processes, and were therefore taken from experimental measurements. The parameters r_o, D_o, and β were chosen in accordance to the experimental dimer properties.[31] Figure 3 shows that the reference data nicely follow a linear slope in the semilogarithmic plot. The parameter S was chosen in a way that allowed the fcc structure to agree with the us-PP LDA result. The equilibrium positions of all other structures are energetically correctly described. Only the bond distances tend to be slightly underestimated for all solid structures. However, the overall agreement is at least good, especially as this parameter set allows one to describe the specificities of the rhombohedral α structure. The bulk moduli are in good agreement with experimental data where available, and in line with the DFT results for structures not observed experimentally. Again the cutoff range of 3.2–3.6 Å was determined by optimizing the melting behavior, which is rather complex in case of arsenic (see Sec. V A for details). It is worth mentioning that to our knowledge the Ga and As potentials are the first analytical models for these elements that reproduce the complex ground-state structures as stable, energetically favored configurations.

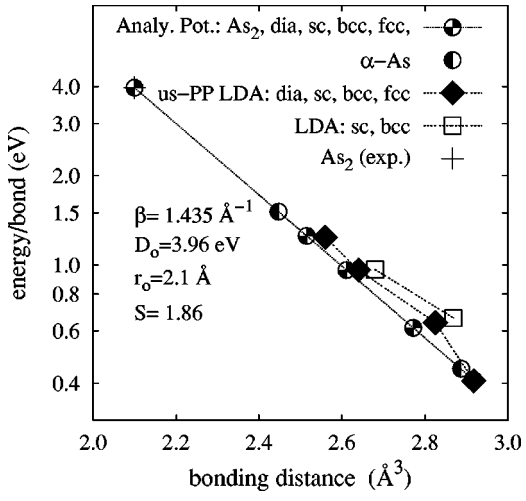

FIG. 3. Semilogarithmic plot of the energy-bond relation for different As structures: Shown are the results of the analytical potential, the us-PP LDA calculations, and literature values of LDA-calculations (Ref. 49). The experimental values for the dimers are taken from Ref. 31.

C. Gallium arsenide

Due to its technological importance GaAs is a very well-characterized material, both theoretically and experimentally. Therefore among III-V semiconductors it has attracted the most attention in high-pressure studies. The currently accepted phase transition sequence on pressure increase at room temperature is GaAs-I (zinc blende) to orthorhombic GaAs-II (Cmcm structure, that can be seen as a distorted $B1$ structure) at about 17 GPa. Upon a further increase of pressure GaAs-II changes to a body-centered-orthorhombic structure GaAs-III (Imm2). Finally, a gradual transformation into a simple hexagonal structure (GaAs-IV) appears at high pressure around 600–800 kbar.[51]

Theoretically, the sc16 structure has been predicted to be stable at modest pressures,[52] but has not been found in experiments. However, another fourfold-coordinated structure, the cinnabar phase, appears in experiments on download from GaAs-II, but in accordance with the DFT calculations is energetically less favored than the sc16 form.[53,54] It therefore remains an open question if the cinnabar phase is an equilibrium structure above 120 kbar pressure or not. Since the total energy neglects zero point contributions and phase transition kinetics, they can only serve as guidelines here.

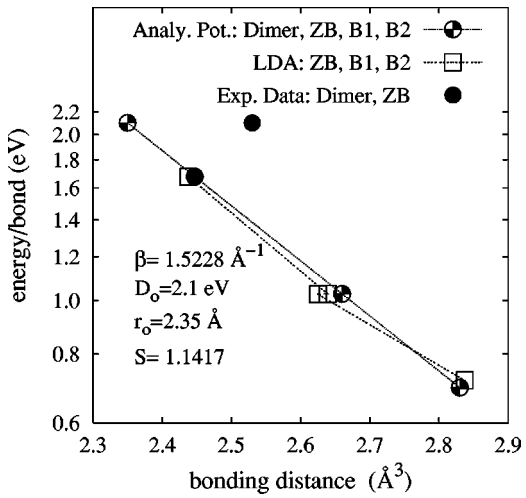

FIG. 4. Semilogarithmic plot of the energy-bond relation for different GaAs structures: Shown are the results of the analytical potential and literature values of LDA calculations (Refs. 57 and 53). The experimental values for the dimer are taken from Ref. 55, and those for the zinc blende structure from Ref. 58.

For deriving the GaAs parameter set we have therefore considered the zinc-blende structure as the only fourfold-coordinated phase. Among the high-pressure forms, we have chosen the $B1$ structure rather than the orthorhombic GaAs-II structures as reference. Modeling the buckling of the Cmcm structure imposes too many constraints on the fitting procedure, which leads to a worse description of the zinc-blende properties. Since the $B1$ and GaAs-II structures are fairly similar, we consider this a justified simplification. As representative of a highly coordinated structure, the metastable $B2$ form has been considered, because none of the thermodynamically stable high-pressure structures has a coordination of eight. Given the fact that a large body of total-energy calculations is accessible in literature, we did not perform any additional DFT calculations on GaAs.

The GaAs dimer is experimentally well characterized. Lemire *et al.*[55] reported a ground state frequency of 215 cm^{-1}, and determined a bond strength of $D_o = 2.06(5)$ eV in accordance with the value of 2.1 eV as given in Huber and Herzberg's data collection.[31] By choosing an experimental bond length of 2.53 Å, however, we were not able to adjust the Pauling relation for the solid structures and therefore changed r_o to a somewhat lower value of 2.35 Å. Even the β parameter as determined from the oscillation frequency, did not allow us to fit the elastic properties of the zinc-blende structure correctly. The value we have chosen corresponds to a ground-state oscillation frequency of 278 cm^{-1}, which is still reasonably close to the experimental number.

All reference data nicely follow a linear relationship in the semilogarithmic plot as depicted in Fig. 4. The angular terms were adjusted by including the elastic moduli for the zinc-blende (ZB) structure GaAs-I into the fitting procedure. Since atomic forces were not calculated for the parameter fitting, the shear modulus was adjusted to the static shear modulus C_{44}^o. The internally relaxed shear modulus and the Kleinman relaxation parameter were calculated afterward, following the procedure given by Nielsen and Martin.[56] It is worth mentioning here that the deformation energy for this shear mode has contributions from the individual bonds and from the bond angles. Even if the ideally deformed structure predicts the correct elastic energy, it is perfectly possible that the internal relaxation leads to a vanishing shear stability characterized by a large Kleinman relaxation parameter ζ.

Table IV gives an overview of the GaAs properties as described by the analytical model. The agreement for all properties is fairly excellent. Only the relaxed shear modulus appears at little bit too low. As before the cutoff parameters were optimized by testing the melting properties (see Sec. V A). The full parameter set is given in Table II.

V. MELTING BEHAVIOR

A. Optimizing the cutoff radii

Since previous GaAs potentials had problems in reproducing even the ground-state structure of the Ga, As and GaAs materials,[59] we placed special emphasis on ensuring that we obtained at least the correct ground-state structure. We used two kinds of test simulations for this. One consisted of heating up crystalline cells until they melted, and subsequently cooling them slowly (over 100 ps to 10 ns) to 0 K, checking that the final structure was higher in the potential energy than the desired ground state. Although this method is good for finding structures with energy minima far below the ground state, it is not good enough to spot minima lying just slightly lower ($\sim$0.1 eV) in energy than the desired state. To test the potential against such local minima, we used simulations of a liquid and solid in equilibrium (the same simulations were also used to determine the melting point, see below). If other energy minima are present, a phase transition to the lower minimum is likely to be initiated at the liquid-solid interface over long time scales.

The cutoff values of the potential were not systematically optimized in the fit of the potential to the different phases. Hence we could somewhat modify them to obtain a better fit to the melting point. Possible cutoff values were limited from below by the nearest-neighbor distance of the fitted structures of materials. The second-nearest neighbor defined an upper limit. The final cutoff was then chosen by testing several values between these limits for melting properties.

The melting point was determined by simulating a box with liquid and crystal phases. The system was first equilibrated at some temperature near the predicted melting point. The development of the phases was observed at several temperatures to see whether the system melted or crystallized. Berendsen pressure control[60] to zero pressure was used in all melting simulations, independently in the x, y, and z dimensions. The number of atoms was 2000–4000 and the simulation time was 200–2000 ps.

The melting point for Ga was found to be 600 ± 100 K. This is clearly higher than the experimental value 303 K,[41] but still not completely unreasonable considering the complex structure of Ga.

For As the experimental melting point is 1090 K (determined at high pressures under an As atmosphere[61]), which is

TABLE IV. Energy and structural parameters of different GaAs phases. Given are experimental values and theoretical results from DFT calculations in comparison to the corresponding numbers as described with the analytical model.

GaAs dimer			Exp. (Ref. 55)	Anal. Pot.
r_o (Å)			2.53(2)	2.35
D_o (eV)			2.06(5)	2.1
ω_o (cm^{-1})			215	278
$GaAs_2$				$B_{ij}=0.9825$
r_o (Å)				2.412
E_{bond} (eV)				−1.821
Zincblende GaAs	scf-LDA (Ref. 57)	scf-LDA (Ref. 53)	(Ref. 58)	$B_{ij}=0.9724$
V (Å^3/f.u.)	44.66	44.14	45.16	45.16
a_o (Å^3)	5.632	5.610	5.653	5.653
r_o (Å^3)	2.438	2.429	2.447	2.447
E_{coh}/f.u. (eV)	(−6.71)	(−6.71)	−6.71	−6.71
E_{bond} (eV)	(−1.677)	(−1.677)	−1.677	−1.677
B (GPa)			74.8	73.3
B'			4.56	4.5
C_{11} (GPa)			118.1	123.6
C_{12} (GPa)			53.2	48.2
C_{44} (GPa)			59.2	39.4
ζ				0.547
C_{44}^0 (GPa)			75.0 (Ref. 56)	73.2
T_{melt} (K)			1513 K	1900(100) K
$B1$				$B_{ij}=0.9152$
V (Å^3/f.u.)	36.76	36.1948		37.64
a_o (Å^3)	5.278	5.251		5.32
r_o (Å^3)	2.639	2.625		2.660
E_{coh}/f.u. (eV)	−6.168	−6.156		−6.168
E_{bond} (eV)	−1.028	−1.026		−1.028
B (GPa)				95.63
B'				4.77
$B2$				$B_{ij}=0.8718$
V (Å^3/atom)	35.16			34.89
a_o (Å^3)	3.276			3.267
r_o (Å^3)	2.837			2.830
E_{coh}/atom (eV)	−5.73			−5.56
E_{bond} (eV)	−0.716			−0.695
B (GPa)				104.9
B'				4.96

higher than the boiling point, 880 K, determined at normal temperature and pressure.[61] Interpreting how this behavior should be reflected within the limited time scale of MD simulations is not straightforward. Nevertheless, we simulated As at 400, 700, 800, and 1200 K. At 400 K the system crystallized. At 700 and 800 K the liquid boiled quickly, but crystallization was also observed. The whole system boiled at 1200 K. Considering the complex experimental behavior, we consider this to be in good agreement with the experiments.

Simulation temperatures of 1700, 1800, 1900, 2000, and 2100 K were used for the GaAs system. With the selected cutoff, the melting point was 1900±100 K, in good agreement with the experimental value of about 1500 K.[62]

The molten GaAs phase was initially stable, but after long simulation times (~1 ns) around or above the melting point, pure As bubbles form in the liquid, leaving the rest of the molten zone in a Ga-rich GaAs phase. This kind of segregation is also believed to occur in the liquid phase of real GaAs.[62]

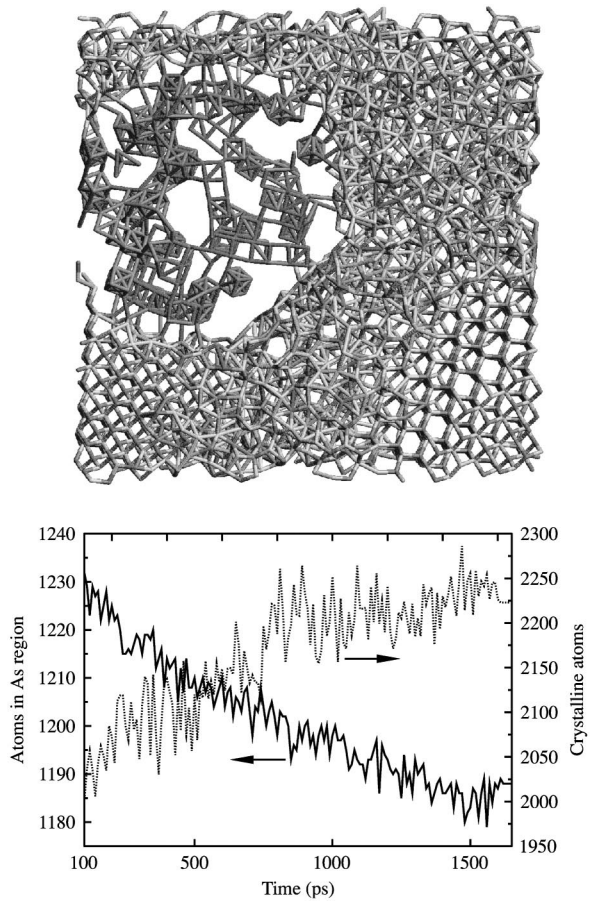

FIG. 5. (a) Structure of amorphous GaAs after melting at 1900 K at 0 pressure and subsequent cooling to 1500 K. The figure is a 15-Å cross section of the whole simulation cell. Only the covalent bonds between atoms are shown, with the half of the bonds closer to As shown by the darker color and the half of the bonds closer to Ga shown by the lighter color. The low-density region on the upper left is a segregated As bubble which has formed during melting. On the lower left and lower right a recrystallized GaAs region has formed. (b) Number of atoms in the As region and crystalline atoms in an equilibration run below the melting temperature of a simulation cell similar to the one in (a). A ''crystalline'' atom is defined here as a fourfold-coordinated As atom with all bonds to Ga atoms, or a fourfold-coordinated Ga atom with all bonds to As atoms. The figure shows how the As bubble shrinks and the crystalline region grows during equilibration.

B. Test of melting and recrystallization properties

In addition to the melting point simulations, we also analyzed the structure of molten and quenched GaAs by a series of simulation where GaAs first became molten starting from random atom positions, and subsequently cooled below the melting temperature in one or several stages.

When GaAs became molten at zero pressure, even only slightly above the melting temperature, we observed that some (but not all) of the As atoms segregated into a separate As phase. This phase obtained a dilute structure with As atoms predominantly in tetrahedral As_4 and cubic As_8 configurations which are weakly bound to each other. The structure of the segregated As is illustrated in Fig. 5(a).

This behavior is in good qualitative agreement with experiments on liquid GaAs, which was reported to be Ga rich unless placed under a high pressure in an As atmosphere.[62,63] In the gas phase over a solid or liquid, Arthur[63] showed that As is predominantly in the form of As_2 and As_4 molecules. Furthermore, he argued that, in a solution, As forms segregated polymerized structures with an estimated number of 10–15 in the As aggregations. Recently, Godlevsky and Chelikowsky reported that they did not observe As clusterization in *ab initio* calculations on liquid GaAs (Ref. 64); however, their simulations were carried out in systems with only 64 atoms and over a few ps. It is not clear whether a segregated As phase can even be expected to form over such a short time scale. We propose that the mixture of As_4 and As_8 bound to each other, which we observe in the liquid GaAs, could be the polymerized structure suggested by Arthur.

When this liquid phase is rapidly cooled below the melting temperature, the As bubbles first remains intact, but in equilibration runs at temperatures around 1300–1500 K over nanosecond time scales we observed that they slowly shrink in size, and the As is absorbed into the surrounding GaAs [see Fig. 5(b)]. The shrinkage is much faster when the cell is under a high pressure, of the order of 10 kbar, as expected from the equilibrium pressures of As over GaAs.[63] At the same time, a crystalline phase starts to form in another part of the simulation cell [Fig. 5(a)], although during this nanosecond time scale it still has some defects in it.

Because the ground state of GaAs in the solid phase is the stoichiometric crystalline state, the observed recrystallization behavior is what would be expected experimentally. Since the correct fourfold-coordinated crystalline structure is obtained here starting from a completely random atom configuration, this also gives us great confidence that our potential does indeed give the right ground-state structure of GaAs. Since long-range interactions are not part of the potential, however, there is of course no energy difference between different packing sequences of {111} planes.[65]

VI. DEFECT PROPERTIES

Defect formation energies were calculated with this analytical potential for a system that was as thermally equilibrated at 600 K, and then slowly cooled down to 0 K at zero pressure. The defect formation was calculated then from the potential energy E_D of the cell containing the defect using the formalism of Qian *et al.*,[66]

$$\begin{aligned}\Omega_D(\mu_G a,\mu_A s) &= \underbrace{E_D - \tfrac{1}{2}(n_{Ga}+n_{As})\mu^{bulk}_{GaAs} - \tfrac{1}{2}(n_{Ga}-n_{As})(\mu^{bulk}_{Ga}-\mu^{bulk}_{As})}_{E'_D} \\ &\quad - \tfrac{1}{2}(n_{Ga}-n_{As})\Delta\mu\,,\end{aligned} \tag{8}$$

where n's are the number of atoms in the cell and μ's the corresponding chemical potential. For thermodynamic reasons $\Delta\mu$ is restricted to the range $-\Delta H_f < \Delta\mu < \Delta H_f$.

The calculations were carried out with a 64-atom cell in order to allow a better comparison with *ab initio* supercell

TABLE V. Defect formation energies of different point defects as calculated with the analytical potential using a 64 atom cell and pressure control. For comparison results of LDA calculations by Northrup and Zhang (Ref. 67) and Pöykkö *et al.* (Ref. 68) are given.

Type	E_D' (eV)	ΔV (Å^3)	E_D' (eV) (Ref. 67)	E_D' (eV) (Ref. 68)
V_{Ga}	2.4	−32	4.55	
V_{As}	2.0	−45		2.33
I_{Ga}	1.1	18	2.14 (I_{Ga}^{+})	
I_{As}	5.9	44	6.14	
Ga_{As}	1.5	1.5	2.74	
As_{Ga}	5.6	26	2.50	2.29
V_{Ga}-V_{As}	3.8	−14	3.54	

calculations. The results are summarized in Table V. The vacancy formation energies are well reproduced and the Ga interstitial I_{Ga} is predicted to be the most stable neutral point defect in agreement with the results of Pöykkö *et al.*,[68] while the As interstitial I_{As} has the highest formation energy, which is predicted by DFT calculations, as well. Among the antisite defects, however, the formation energy of As_{Ga} is poorly described.

VII. SURFACE PROPERTIES

The GaAs(001) surface is known to have many reconstructions depending on growth conditions.[69,70] Probably the most relevant of them—from the point of view of molecular beam epitaxy—are the As-terminated 2×4 surface structures. There is experimental evidence of the $\alpha(2\times4)$, $\beta(2\times4)$, $\beta2(2\times4)$, and $\gamma(2\times4)$ reconstructions. In addition, a $c(4\times4)$ structure has been reported.

The ability of the current potential to describe the properties of the GaAs(001) surface was investigated by calculating the minimum-energy configurations of the As-rich surface reconstructions $\alpha(2\times4)$, $\beta(2\times4)$, $\beta2(2\times4)$, $\gamma(2\times4)$, and $c(4\times4)$. Energy minimization was performed using the conjugate gradient technique, with the initial atom positions taken from the literature (see, e.g., Ref. 71). The simulation systems consisted of $12\times12\times5$ unit cells with the number of atoms between 2772 and 2880 (depending on the reconstruction) with the bottom layer of the atoms fixed. Qualitatively, the resulting geometries were in agreement with the calculations in the literature. However, the current potential gives a value of 3.2 Å for the surface As dimer bond length for the $\alpha(2\times4)$, $\beta(2\times4)$, and $\beta2(2\times4)$ reconstructions while the latest *ab initio* calculations indicate a value in the range of 2.5 to 2.6 Å.[71]

As the Tersoff parametrization of Sayed *et al.*[12] for GaAs is known to produce unstable surfaces,[72] the stability of surfaces described by the current potential was tested by MD simulations of the above-mentioned reconstructions at finite temperatures. The systems were simulated for 5 ps in a constant temperature mode, after which they were slowly cooled to zero temperature with a cooling rate of 0.01 K/fs. All the reconstructions with low As coverages [$\alpha(2\times4)$, $\beta(2\times4)$, and $\beta2(2\times4)$] were stable up to about 800 K, above which defects began to form on the surface. The structures with high As content [$\gamma(2\times4)$ and $c(4\times4)$] were unstable even at low temperatures. The topmost As dimers began to dissociate and desorb at 100 K in these surface structures.

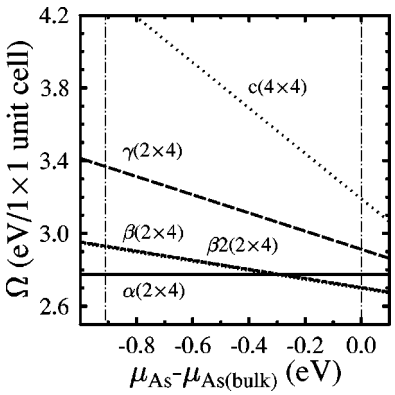

FIG. 6. Surface energies of the reconstructions studied in this work. Note that reconstructions $\beta(2\times4)$ and $\beta2(2\times4)$ have nearly equal energies. Vertical lines indicate the allowed range of μ_{As}. The value used for $\mu_{(Asbulk)}$ was 2.965 eV as obtained for α-As using the current potential.

These results indicate that the As-As interaction is not well optimized for a description of As-terminated surfaces. This conclusion is supported by the further observation that the surface energies of the high-As-coverage reconstructions were too large compared to the energies of the $\alpha(2\times4)$, $\beta(2\times4)$, $\beta2(2\times4)$ surfaces. In Fig. 6 we show the formation energies of the reconstructions studied in this work as a function of the chemical potential of the As atom reservoir μ_{As}. The formation energy Ω is calculated by the equation[71]

$$\Omega = U - n_{Ga}E_{GaAs} - \Delta n\,\mu_{As}, \tag{9}$$

where U is the potential energy of the surface configuration, n_{Ga} is the number of Ga atoms in the system, and E_{GaAs} is the formation energy per molecule of GaAs. Δn is the stoichiometry of the system [0, 1/4, 1/4, 5/4, and 1/2 per 1×1 unit cell for $\alpha(2\times4)$, $\beta(2\times4)$, $\beta2(2\times4)$, $c(4\times4)$, and $\gamma(2\times4)$, respectively]. The allowed range of μ_{As} is $\mu_{As(bulk)}-\Delta H_f<\mu_{As}<\mu_{As(bulk)}$, where ΔH_f is the formation energy of GaAs from bulk Ga and As. By using the current potential we get the limits 2.054 eV$<\mu_{As}<$2.965 eV.

In the literature,[71,73–75] the sequence of stable structures of an As-terminated GaAs(001) surface when going from Ga-rich to As-rich environment (from small to large μ_{As}) is generally observed to be $\alpha(2\times4)\rightarrow\beta(2\times4)/\beta2(2\times4)\rightarrow\gamma(2\times4)\rightarrow c(4\times4)$. The current potential predicts so large formation energies for the $\gamma(2\times4)$ and $c(4\times4)$ reconstructions that they would not be stable in the allowed range of the As chemical potential.

In order to obtain a more realistic dimer bond length and formation energies some test runs were performed by scaling the As-As cutoff radius. However, even by decreasing the cutoff by 0.4 Å resulted in a dimer bond length of 2.9 Å which is still too large. In addition to this, the effect of the potential parameter $\mu_{As\text{-}As}$ for the As-As interaction in Eq. (4) on the As dimer bond length was studied. By increasing

the parameter, the dimer bond length decreases and the formation energies of the As-rich reconstructions become smaller, as desired. However, these manipulations affect the properties found for the pure As structures, especially the phase stability of α-As. Since we wanted to design a general parameter set, no further adjustments of the arsenic parameters toward a better description of surface properties were done. However, this is in principle possible if pure arsenic structures do not play a role in the specific application of the potential.

VIII. CONCLUSIONS

We have presented an analytical potential for modeling Ga, As, and GaAs using a short-ranged bond-order algorithm. The potential describes different dimer properties and several solid structures of the pure elements and the compound including metastable configurations. Most importantly, the complicated α-As and α-Ga structures are reproduced as thermodynamically most stable phases which was verified by investigations of the melting behavior. For Ga, As, and GaAs the melting points are quite well reproduced by optimization of the cutoff function. Point defect properties were checked and compared to LDA results from literature. Except for the As antisite defect, all defect properties are in line with LDA calculations from the literature. Testing the surface properties resulted in a similar picture, namely, a reasonable agreement for those reconstruction with little As coverage. Surfaces with As-rich configurations, however, are not realistically described. In a first application the structure of molten GaAs has been investigated. Our simulations reveal the segregation of arsenic in a polymeric structure, which corresponds to experimental findings.

In conclusion, this is to our knowledge the only interatomic potential that describes the structure and bonding of Ga, As, and GaAs within one analytical form, and therefore allows atomistic computer simulations of a wide range of materials problems related to GaAs. These include crystallization from melt, defect formation and clustering in the bulk, as well as thermomechanical properties of Ga, As, and GaAs. The potential in the present form, however, does not seem to be suitable for simulations of surface growth processes where As-rich surface reconstructions play a role.

ACKNOWLEDGMENTS

The research was supported by the Academy of Finland under Project Nos. 46788 and 51585. Grants of computer time from the Center for Scientific Computing in Espoo, Finland are gratefully acknowledged. This work was supported by the Academy of Finland, Research Centre for Computational Science and Engineering, Project No. 44897 (Finnish Centre of Excellence Program 2000-2005). One of us (K.A.) was also partly supported by the U.S. Department of Energy, Basic Energy Sciences, under Grant No. DEFG02-91ER45439, and by the U.S. Department of Energy through the University of California under Subcontract No. B341494.

APPENDIX: FIT OF A REPULSIVE POTENTIAL

In applications where one needs to take high-energetic ($E_{kin} \gg 10$ eV) collisions between atoms into account, it is necessary to modify the repulsive part of the potential to realistically describe such collisions. To this end, we first derive an accurate repulsive pair potential for a dimer using a density-functional theory method.[76] We then construct a total potential V_{Tot} using

$$V_{Tot}(r) = V_R(r)[1 - F(r)] + [V_{Eq}(r)]F(r), \qquad \text{(A1)}$$

where V_{Eq} is the individual bond energy described in the main text, and the Fermi function

$$F(r) = \frac{1}{1 + e^{-b_f(r - r_f)}}. \qquad \text{(A2)}$$

The values of the constants b_f and r_f are chosen such that the potential is essentially unmodified at the equilibrium and longer bonding distances, and that a smooth fit at short separations with no spurious minima is achieved for all realistic coordination numbers of the atoms (1–12). We have also checked that these fits give a realistic value for the effective threshold displacement energy in GaAs.[77]

Using this approach we obtained $r_f = 1.2$ Å and $b_f = 12.01/$Å for the Ga-Ga interactions, and $r_f = 1.0$ Å and $b_f = 12.01/$Å for Ga-As and As-As interactions. These same values also give a smooth fit to the Ziegler-Biersack-Littmark universal repulsive potential.[78]

*Author to whom correspondence should be addressed. Present address: Institut für Materialwissenschaft, TU Darmstadt, D-64287 Darmstadt, Germany. Email address: albe@tu-darmstadt.de.

[1] J. W. Mayer and S. S. Lau, *Electronic Materials Science For Integrated Circuits in Si and GaAs* (MacMillan, New York, 1990).

[2] M. Hong, J. Kwo, A.R. Kortan, J.P. Mannaerts, and A.M. Sergent, Science **283**, 1897 (1999).

[3] H. Hausmann, A. Pillukat, and P. Ehrhart, Phys. Rev. B **54**, 8527 (1996).

[4] M. C. Ridgway, C. J. Glover, E. Bezakova, A. P. B. G. J. Foran, and K. M. Yu, Nucl. Instrum. Methods Phys. Res. B **148**, 391 (1999).

[5] A. Turos, A. Stonert, B. Breeger, E. Wendler, W. Wesch, and R. Fromknecht, Nucl. Instrum. Methods Phys. Res. B **148**, 401 (1999).

[6] T. Diaz de la Rubia, R.S. Averback, R. Benedek, and W.E. King, Phys. Rev. Lett. **59**, 1930 (1987).

[7] M. Kitabatake, J. Appl. Phys. **73**, 3183 (1993).

[8] M.O. Pedersen, I.A. Bönicke, E. Lægsgaard, I. Stensgaard, A. Ruban, J.K. Norskov, and F. Besenbacher, Surf. Sci. **387**, 86 (1997).

[9] K. Nordlund, M. Ghaly, R.S. Averback, M. Caturla, T. Diaz de la Rubia, and J. Tarus, Phys. Rev. B **57**, 7556 (1998).

[10] T. Ito, K. Khor, and S. Das Sarma, Phys. Rev. B **41**, 3893 (1989).

[11] R. Smith, Nucl. Instrum. Methods Phys. Res. B **67**, 335 (1992).

[12] M. Sayed, J.H. Jefferson, A.B. Walker, and A.G. Gullis, Nucl. Instrum. Methods Phys. Res. B **102**, 232 (1995).
[13] K. Nordlund and A. Kuronen, Nucl. Instrum. Methods Phys. Res. B **159**, 183 (1999).
[14] D. Conrad and K. Scheerschmidt, Phys. Rev. B **58**, 4538 (1998).
[15] S. Kodiyalam, A. Chatterjee, I. Ebbsjo, R. K. Kalia, H. Kikuchi, A. Nakano, J. P. Rino, and P. Vashishta, in *Microcrystalline and Nanocrystalline Semiconductors*, edited by M. J. Sailor *et al.*, Symposia Proceedings No. 536 (Materials Research Society, Warrendale, PA, 1999), pp. 545–50.
[16] F. Streitz and J. Mintmire, Phys. Rev. B **50**, 11 996 (1994).
[17] D. Brenner, Phys. Rev. Lett. **63**, 1022 (1989).
[18] J. Tersoff, Phys. Rev. B **49**, 16 349 (1994) (and references therein).
[19] D.W. Brenner, Phys. Rev. B **42**, 9458 (1990); **46**, 1948 (1992).
[20] K. Khor and S. Das Sarma, Phys. Rev. B **38**, 3318 (1988).
[21] P. Alinghian, S. Nishitani, and D. Pettifor, Philos. Mag. B **69**, 889 (1994).
[22] I. Oleinik and D. Pettifor, Phys. Rev. B **59**, 8500 (1999).
[23] D. Pettifor, *Bonding and Structure of Molecules and Solids* (Oxford Science Publications, Oxford, 1995).
[24] R. Jones and O. Gunnarsson, Rev. Mod. Phys. **61**, 689 (1989).
[25] M.C. Payne, M.P. Teter, D.C. Allan, T.A. Arias, and J.D. Joannopoulos, Rev. Mod. Phys. **64**, 1045 (1992).
[26] D. Ceperley and B. Alder, Phys. Rev. Lett. **45**, 566 (1980).
[27] J. Perdew and A. Zunger, Phys. Rev. B **23**, 5048 (1981).
[28] F. Birch, J. Geophys. Res. **83**, 1257 (1978).
[29] K. Albe, Phys. Rev. B **55**, 6203 (1997).
[30] W. H. Press, S. A. Teukolsky, W. T. Vetterling, and B. P. Flannery, *Numerical Recipes in C; The Art of Scientific Computing*, 2nd ed. (Cambridge University Press, New York, 1995).
[31] K. Huber and G. Herzberg, *Constants of Diatomic Molecule* (Van Nostrand Reinhold, New York, 1979).
[32] J. Donohue, in *The Structures of Elements*, edited by J. W. Sons (Wiley, New York, 1974).
[33] C. Kittel, *Introduction to Solid State Physics*, 5th ed. (Wiley, New York, 1976).
[34] K. Lyall and J. Cochran, Can. J. Phys. **49**, 1075 (1971).
[35] L. Bosio, J. Chem. Phys. **68**, 1221 (1978).
[36] K. Balasubramanian, J. Phys. Chem. **94**, 7764 (1990).
[37] I. Shim, K. Mandix, and K. Gingerich, J. Phys. Chem. **95**, 5435 (1991).
[38] K.K. Das, J. Phys. B **30**, 803 (1997).
[39] T. Gosh, K. Tanaka, and Y. Mochiuzuki, Theochem-J. Mol. Struct. **451**, 61 (1998).
[40] M. Bernasconi, G. Chiarotti, and E. Tosatti, Phys. Rev. B **52**, 9988 (1995).
[41] L. Bosio, J. Chem. Phys. **68**, 1221 (1978).
[42] D.A. Walko and I.K. Robinson, Phys. Rev. Lett. **81**, 626 (1998).
[43] X. Gong, G. Chiarotti, M. Parinello, and E. Tosatti, Phys. Rev. B **17**, 14277 (1991).
[44] L. Mattheiss, D. Hamann, and W. Weber, Phys. Rev. B **34**, 2190 (1986).
[45] R. Needs, R. Martin, and O. Nielsen, Phys. Rev. B **33**, 3778 (1986).
[46] R. Needs, R. Martin, and O. Nielsen, Phys. Rev. B **35**, 9851 (1987).
[47] H. Beister, K. Strössner, and K. Syassen, Phys. Rev. B **41**, 5535 (1990).
[48] T. Kikegawa and H. Iwasaki, J. Phys. Soc. Jpn. **56**, 3417 (1987).
[49] T. Sasaki, K. Shindo, and K. Niizeki, Solid State Commun. **67**, 569 (1988).
[50] K. Chang and M. Cohen, Phys. Rev. B **33**, 7371 (1986).
[51] M. McMahon and R. Nelmes, Phys. Rev. Lett. **78**, 3697 (1997).
[52] A. Mujica, R.J. Needs, and A. Munoz, Phys. Rev. B **52**, 8881 (1995).
[53] A. Mujica and A. Munoz, Phys. Rev. B **57**, 1344 (1998).
[54] A.A. Kelsey, G.J. Ackland, and S.J. Clark, Phys. Rev. B **57**, 2029 (1998).
[55] G. Lemire, G. Bishea, S. Heidecke, and M. Morse, J. Chem. Phys. **92**, 121 (1990).
[56] O. Nielsen and R.M. Martin, Phys. Rev. B **32**, 3792 (1985).
[57] A.A. Demkov and O.F. Sankey, Phys. Rev. B **55**, 6904 (1997).
[58] D. Dunslan, in *Properties of GaAs*, edited by M. Brozel and G. Stillmann (Inspec, London, 1996).
[59] K. Nordlund, J. Nord, J. Frantz, and J. Keinonen, Comput. Mater. Sci. **18**, 283 (2000).
[60] H.J.C. Berendsen, J.P.M. Postma, W.F. van Gunsteren, A. DiNola, and J.R. Haak, J. Chem. Phys. **81**, 3684 (1984).
[61] R. Bellissent, C. Bergman, R. Ceolin, and J. Gaspard, Phys. Rev. Lett. **59**, 661 (1987).
[62] J.A.V. Vechten, Phys. Rev. B **7**, 1479 (1973).
[63] J.R. Arthur, J. Phys. Chem. Solids **28**, 2257 (1967).
[64] V. Godlevsky and J.R. Chelikowsky, J. Chem. Phys. **109**, 7312 (1998).
[65] J. P. Hirth and J. Lothe, *Theory of Dislocations*, 2nd ed. (Krieger, Malabar, FL, 1992).
[66] G.-X. Qian, R.M. Martin, and D.J. Chadi, Phys. Rev. B **38**, 7649 (1988).
[67] J.E. Northrup and S. Zhang, Phys. Rev. B **47**, 6791 (1993).
[68] S. Pöykkö, M. Puska, and R. Nieminen, Phys. Rev. B **53**, 3813 (1996).
[69] C.B. Duke, Chem. Rev. **96**, 1237 (1996).
[70] K. Jacobi, J. Platen, and C. Setzer, Phys. Status Solidi B **218**, 329 (2000).
[71] M.A. Salmi, M. Alatalo, T. Ala-Nissilä, and R.M. Nieminen, Surf. Sci. **425**, 31 (1999).
[72] A. Kuronen, J. Tarus, and K. Nordlund, Nucl. Instrum. Methods Phys. Res. B **153**, 209 (1999).
[73] J.E. Northrup and S. Froyen, Phys. Rev. Lett. **71**, 2276 (1993).
[74] N. Moll, A. Kley, and E.P.M. Scheffler, Phys. Rev. B **54**, 8844 (1996).
[75] M. Haugk, J. Elsner, and T. Frauenheim, J. Phys.: Condens. Matter **9**, 7305 (1997).
[76] K. Nordlund, N. Runeberg, and D. Sundholm, Nucl. Instrum. Methods Phys. Res. B **132**, 45 (1997).
[77] K. Nordlund, J. Peltola, J. Nord, J. Keinonen, and R.S. Averback, J. Appl. Phys. **90**, 1710 (2001).
[78] J. F. Ziegler, J. P. Biersack, and U. Littmark, *The Stopping and Range of Ions in Matter* (Pergamon, New York, 1985).